IEEE Access
Multidisciplinary ⋮ Rapid Review ⋮ Open Access Journal

Received February 15, 2020, accepted March 1, 2020, date of publication March 10, 2020, date of current version March 18, 2020.

Digital Object Identifier 10.1109/ACCESS.2020.2979409

An Adaptive Peak Detection Method for Inspection of Breakages in Long Rails by Using Barker Coded UGW

XIAOYUAN WEI[1,2,3], YUAN YANG[1,2], JESÚS UREÑA[3], (Senior Member, IEEE), JIAXUAN YAN[1,2], AND HAOZHEN WANG[1,2]

[1]Department of Electronic Engineering, Xi'an University of Technology, Xi'an 710048, China
[2]Shaanxi Key Laboratory of Complex System Control and Intelligent Information Processing, Xi'an 710048, China
[3]Department of Electronic, University of Alcalá, 28805 Alcalá de Henares, Spain

Corresponding author: Yuan Yang (yangyuan@xaut.edu.cn)

This work was supported in part by the National Natural Science Foundation of China under Grant 51477138, in part by the Key Research and Development Program of Shaanxi Province under Grant 2017ZDXM-GY-130, in part by the Xi'an City Science and Technology Project under Grant 2017080CG/RC043(XALG009), in part by the Xi'an University of Technology Outstanding Doctoral Innovation Fund Project under Grant 310-252071707, and in part by the Spanish Ministry of Sciences and Innovation (MICROCEBUS Project) under Grant TIN2018-095168-B-C51.

ABSTRACT For a broken rail detection system based on ultrasonic guided waves (UGW), the multimodal and dispersion of UGW degrade signal-to-noise ratio (SNR) and range resolution. To improve SNR of the received signals and range resolution, the pulse compression technique based on 13-bit Barker code is presented in this work. Through a PSpice model of the pitch-catch setup, as well as performing field tests, it is shown that coded UGW signals can efficiently improve SNR by 5 dB and have strong noise immunity. As the detection distance increases, the mainlobe width increases linearly while the sidelobe peak levels remain basically unchanged. In addition, to correctly and quickly identify the corresponding transmissions at the receivers, an adaptive peak detection algorithm is proposed, which is based on a digital bandpass tracking filter, moving averaging filters and Hilbert transform. By using some field tests under different detection distances, it is found that compared to the previous works, the proposed adaptive peak detection algorithm has stronger robustness and better anti-noise performance. In addition, the proposed method is easy to integrate into a real-time detection system by proper software design.

INDEX TERMS Peaks detection, barker code, pulse compression, long rail breakages detection, UGW.

I. INTRODUCTION

Ultrasonic Guided Waves (UGW) were widely used in the last years in various applications of defects detection in systems such as concretes, pipelines, and rails [1]–[3]. Essentially, UGW belongs to a mechanical wave and has some inherent properties including long-range coverage, low detection frequency, and high inspection efficiency. In recent years, broken rail detections of continuous welded rails (CWR) based on UGW have achieved rapid development [4], [5]. A broken rail real-time detection system based on UGW was developed in [6]. In view of the UGW energy attenuation, UGW dispersion and multimode propagation in long rails, the amplitude and signal-to-noise ratio (SNR) of the received signal are low in practice. In addition, ambient factors, like temperature, humidity, and rain, will further aggravate the reduction of SNR. To obtain a good defect characterization and localization in long rails broken detection based on UGW, high SNR of the received signals is required.

Taking into account the previous considerations, some limitations still exist though these improvements in hardware development and signal processing were performed in [7]–[11]. The amplitude increment of the emitted signal is restricted due to the limitation of excitation voltage of piezoelectric ultrasonic transducers [9]. Besides, some dispersion compensation approaches were utilized to better obtain characteristic information from the received signals [10], [11]. It is pointed out that the amplitude enhancement of the received signal is still limited even if the dispersion effect could be completely eliminated. Initially, to effectively

The associate editor coordinating the review of this manuscript and approving it for publication was Wei Wang.

extend the transmission time what enhanced SNR, encoding excitation technique was used in some medical applications based on ultrasonic detection technique. Zhang *et al.* [12] utilized a Barker coded excitation in long bone detection to generate UGW and it was found that Barker coded excitation made the SNR of the received signal increase by 6.64 dB. To improve ultrasonic imaging quality in terms of axial resolution and SNR, a new Barker coded excitation based on a linear chirp carrier was proposed in [13]. Hereafter, the encoding excitation technique was introduced in other ultrasonic detection applications. A signal processing approach of exploiting chirp excitation in Lamb waves was proposed in [14] to achieve defect detection and localization. Yucel *et al.* [15] compared the maximal length sequences and linear chirp excitation for achieving high-resolution UGW response. Li and Zhou *et al.* [16] proposed the use of P4 Polyphase sequences to code ultrasound in a non-destructive testing system based on air-coupled piezoelectric transducers. For the purpose of improving high-voltage impulses used in track circuits, encoding excitations based on Kasami sequences and LS codes were compared in [17]. However, the chirp excitation requires complex circuits and the generation of excitation based on P4 Polyphase sequences is also complex. Compared with Barker code, Kasami sequences have a higher auto-correlation range sidelobe level. It is worth noting that Barker code has the lowest auto-correlation range sidelobe level among all binary codes of the same length and just needs a single transmission. Additionally, it has a low requirement for hardware. Thence, the encoding excitation technique based on Barker code used in a long rail broken detection system using UGW is utilized in this paper.

For a detection system using encoded excitation, the selection of bits and carrier cycles for Barker code will have an influence on SNR and duration of the received signal. Generally, pulse compression based on Barker code is accomplished by using a matched filter in the received end. Some sidelobes will appear in the output results of the matched filter, which is from the effects of UGW dispersion in rails, effects of the used modulation techniques, bandwidth constraints, multi-path, and noise. Owing to these sidelobes, the signal obtained through the matched filter is not perfect. Therefore, it is vital to adopt peaks detection approaches for the correct identification of maximum peaks. In previous works, most maximum detection systems were based on a fixed threshold [18], [19], but the disadvantage of using fixed thresholds derived from the difficulty of adjusting its value to detect signals under variable energy changing. To overcome the problem, a dynamic threshold was employed to detect maxima [20], which can fit at every moment to the energy of the received signal, existing noise, and other factors. Then a further investigation about the maxima identification was found in the medical field for the detection of electrocardiogram (ECG) QRS complex [21]–[23]. An algorithm using differentiation at the pre-processing stage combined with a dynamic threshold to detect R peaks was proposed in [21]. Manikandan and Soman [22] presented a new R-peak

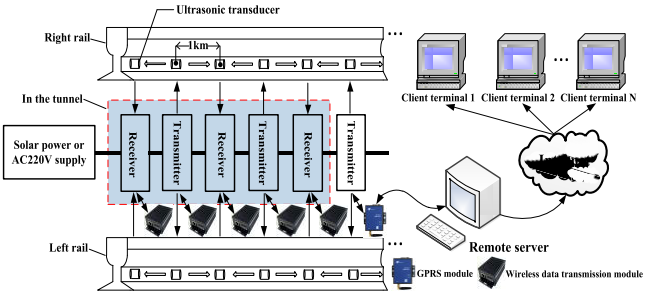

FIGURE 1. Structure diagram of a broken rail real-time detection system based on UGW [6].

detector based on Shannon energy envelope, Hilbert transform, and moving average filter. An automated R-peaks detection method based on wavelet transform and Hilbert transform was described in [23]. Furthermore, by using discrete wavelet transform and Hilbert transform, a novel adaptive peak detection algorithm for track circuits based on encoded transmissions was shown in [24]. But these algorithms either require some amplitude thresholds or have high complexity which cannot meet the real-time requirement of the broken rail detection systems based on UGW. Given these considerations aforementioned, this work proposes an adaptive peak detection algorithm for long rails broken detection using UGW, based on a digital bandpass filter (DBTF), a triangle filter, and Hilbert transform. It is shown that Barker coded UGW signals can efficiently improve SNR by 5 dB and have a strong immunity to noise. In addition, 13-bit Barker code modulated by using 20 carrier cycles can well satisfy requirements of SNR and range resolution of the detection of breakages in long rails. Compared to the previous works, the proposed adaptive peaks detection algorithm has stronger robustness and better anti-noise performance.

The rest of this paper is organized as follows: Section 2 describes the PSpice model of a pitch-catch setup, the Barker encoding, and the pulse compression scheme, as well as the proposed adaptive peak detection algorithm; Section 3 presents, both, simulated and experimental results and discussions; finally, some conclusions are outlined in Section 4.

II. MATERIALS AND METHODS

Generally, the pitch-catch mechanism is often used in ultrasonic detection systems especially in structural health monitoring (SHM). Fig. 1 shows a broken rail real-time detection system based on UGW. The transmitter and the receiver are separated by 1 km and the detection system performs the crack assessment based on the characteristics of the received signals.

The characterized UGW signal will be transmitted every one minute. If the characterized signal is not received, an alarm will be generated. Then, this alarm information is sent to a GPRS module by wireless data transmission modules inside tunnels or other locations with no GPRS signal coverage; finally, it is transmitted to a remote server

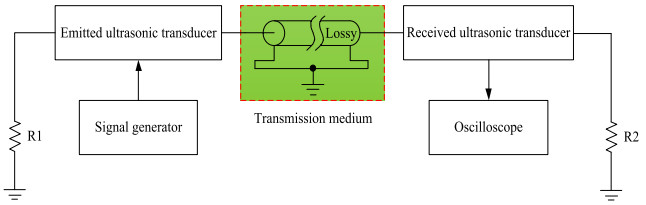

FIGURE 2. Schematic diagram of the PSpice model of a pitch-catch setup.

by GPRS modules. To obtain a good defect characterization and localization, high SNR of the received signals and high range resolution are required.

A. PSPICE MODEL OF THE PITCH-CATCH SETUP

Sandwiched piezoelectric ultrasonic transducers (SPUTs) are usually used in long-range ultrasonic detection. This is due to its advantages like high power, low cost, and easy to manufacture according to design requirements. It mainly consists of a front mass, a back mass, a piezoelectric ceramic stack, metal electrodes, and a high strength prestressed bolt. To perform transient analysis for SPUTs under different encoding excitations, a PSpice model of the pitch-catch setup is involved, as shown in Fig. 2. The PSpice model was established in [26] based on one-dimensional wave and transmission line theories.

It composes of an emitted ultrasonic transducer, a received ultrasonic transducer, transmission medium, a signal generator, and an oscilloscope. Since the back mass of SPUTs is in contact with the air and the front mass is in contact with the web of rails, the air load is taken into consideration to model the acoustic load of the back mass in a SPUT. The resistances *R1* and *R2* denote air load and then the air load can be calculated as follows [25]:

$$R1 = R2 = \rho_1 v_1 A_1 \tag{1}$$

Here, $\rho_1 = 1.293\ \mathrm{kg/m^3}$ is the air density, $v_1 = 340$ m/s is the sound speed in the air, $A_1 = 1075.21\mathrm{mm}^2$ indicates the cross-sectional area of the back mass. Hence, it can be obtained that the resistances $R1{=}R2{=}0.472\ \Omega$. Here, the acoustic lossy transmission line is used to model the transmission medium (CHN60 Rail). The acoustic lossy transmission line includes four parameters as follows [26]:

$$R = \frac{\omega L}{Q_{\mathrm{m}}}, \quad L = A\rho, \mathrm{G{=}0}, \quad \mathrm{C} = \frac{1}{A\rho v_t^2} \tag{2}$$

where R is the resistance per unit length in Ω/m, L is the inductance per unit length in $\mathrm{H/m}$, G is the conductance per unit length in $\mathrm{S/m}$, and C is the capacitance per unit length in $\mathrm{F/m}$. Additionally, Q_{m} represents the mechanical quality factor, A indicates the cross-sectional area, ρ is the material density, v_{t} is the sound speed of longitudinal waves and ω is detection angular frequency. The material parameters of CHN60 Rail are listed in Table 1.

TABLE 1. The material parameters of CHN60 rail used in the simulation.

parameters	A (cm^2)	ρ ($\mathrm{kg/m}^3$)	v_{t} (m/s)	Q_{m}
value	77.45	7850	5790	100

TABLE 2. Barker codes of different bits.

Number of bits	Barker code
2	+1, -1 or -1, +1
3	+1, +1, -1
4	+1, +1, +1, -1 or +1, +1, -1, +1
5	+1, +1, +1, -1, +1
7	+1, +1, +1, -1, -1, +1, -1
11	+1, +1, +1, -1, -1, -1, +1, -1, -1, +1, -1
13	+1, +1, +1, +1, +1, -1, -1, +1, +1, -1, +1, -1, +1

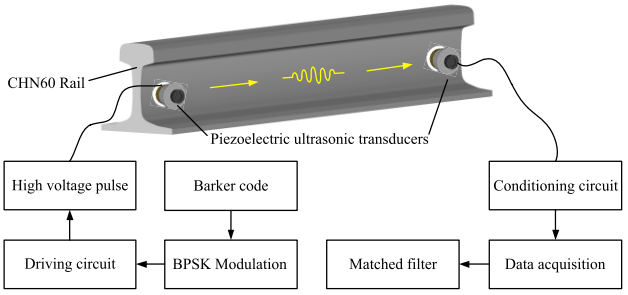

FIGURE 3. Block diagram of the pitch-catch setup based on Barker code.

B. BARKER CODE ENCODING AND PULSE COMPRESSION SCHEME

Barker code is a kind of binary sequences that can be expressed as

$$B[N] = [c_0, c_1, \ldots, c_{N-1}], \quad c_i \in \{-1, +1\} \tag{3}$$

The autocorrelation function (ACF) is [27]

$$\Psi_{\mathrm{AA}}[n] = \begin{cases} N, & n = 0 \\ 0\ or \pm 1, & n \neq 0 \end{cases} \tag{4}$$

From (3), the peak of the autocorrelation is N, and the sidelobe level (SLL) falls between +1 and -1. Note that good ACF is very helpful for the identification of correlation peaks at the receiver. The length N takes values that can be 2, 3, 4, 5, 7, 11, and 13 and cannot be greater than 13 in practice. The Barker codes of different bits are listed in Table 2.

The received signal in a broken rail detection system based on UGW can be mathematically expressed as

$$y(t) = e(t) * h(t) + n(t) \tag{5}$$

where $*$ is the convolution operator, $e(t)$ is excitation pulse, $h(t)$ is system transfer function, $y(t)$ is received signal, and $n(t)$ is additive noise. To better illustrate the process of encoding and decoding of Barker code, a block diagram of the pitch-catch setup is shown in Fig. 3.

Actually, Barker code cannot be used directly to excite a SPUT, since its baseband spectrum does not match with the bandwidth of SPUTs. Hence, it is modulated with a carrier using the BPSK modulation technique. The transmitted signal $e[n]$ can be obtained as [13]:

$$e[n] = v[n] * c[n] \tag{6}$$

where $v(n)$ represents the sample sequence of the carrier denoted as $v(t)$, and $c[n]$ is the oversampled Barker code sequence expressed by

$$c[n] = \sum_{k=0}^{N-1} c_k \delta[n - kT_N f_s] \tag{7}$$

Here, $\{c_k = \pm 1, k = 0, 1, \ldots, N-1\}$ is the original Barker code sequence before oversampling, $T_N = N_c/f_0$ is the chip duration of Barker code, N_c indicates cycles of the selected carrier and f_s is system sample frequency. The total duration of the Barker coded sequence is $T = NT_N$.

It is important to note that the excitation voltage of SPUTs used in long-range detection is as high as thousands of volts. From the perspective of the low complexity of hardware and low cost, the square wave signal $v(t)$ is chosen as the carrier in this paper.

$$v(t) = \frac{4}{\pi}\left[\begin{array}{l}\sin(2\pi f_0 t) + \frac{1}{3}\sin(6\pi f_0 t) + \cdots \\ +\frac{1}{n_1}\sin(2n_1\pi f_0 t) + \cdots\end{array}\right], \ 0 \le t \le T_N \tag{8}$$

Here, f_0 is the frequency of an excitation signal. Taking a 13-bit Barker code with $N_c = 1$ as an example, the encoding process is shown in Fig. 4.

Long-range rail detection is different from small range inspection such as long bone detection since it aims at obtaining SNR as high as possible. Currently, the typical methods of pulse compression include matched filter and mismatched filter. The mismatched filter can achieve lower SLLs at the cost of reducing SNR. For the case of a matched filter, its transfer function $H_1(\omega)$ can be obtained as [28]:

$$H_1(\omega) = k_1 E^*(\omega)\exp(-j\omega t_0) \tag{9}$$

where k_1 is the normalized amplitude constant and $E^*(\omega)$ is the complex conjugate of $E(\omega)$.

Through the inverse Fourier transform, the following equations can be achieved

$$h_1(t) = k_1 e(t_0 - t) \tag{10}$$

From (10), the impulse response function $h(t)$ of the matched filter is obtained by shifting t_0 the flipped version $e(-t)$ of the excitation signal $e(t)$. Thus, the pulse compression signal $d(t)$ can be given as

$$d(t) = y(t) * h_1(t) \tag{11}$$

For the performance evaluation of encoding transmission, two metrics are used which include mainlobe width (MLW)

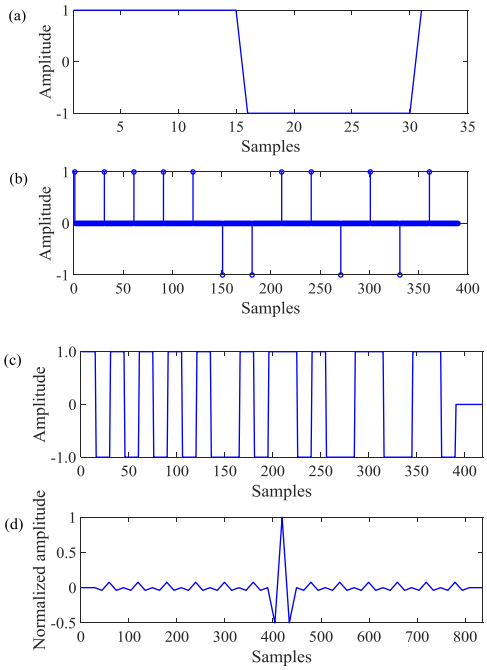

FIGURE 4. The Barker code encoding process, (a) sampled square wave as the carrier, (b) oversampled 13-bit Barker code, (c) modulated Barker code, and (d) its autocorrelation curve.

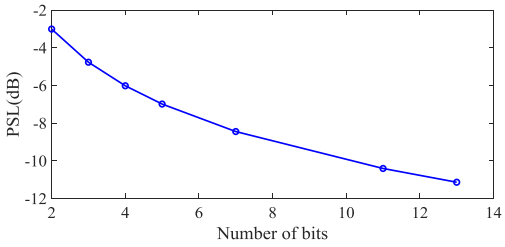

FIGURE 5. The corresponding PSL values of Barker codes of different bits.

and peak sidelobes level (PSL). The PSL formula in decibels can be given as [29]

$$PSL = 10\log\left[\frac{\max(A_{sidelobe})}{\max(A_{mainlobe})}\right] \tag{12}$$

Here, A_{sidelobe} and A_{mainlobe} represent peak values of sidelobes and mainlobes in correlation results, respectively. In addition, MLW can be defined as

$$MLW = t_2 - t_1 \tag{13}$$

Here, $[t_1, t_2]$ denotes the mainlobe width. In practice, MLW determines the inspection resolution.

In light of Table 2 and (12), the corresponding PSL values are obtained and shown in Fig. 5. According to Fig.5, it is shown that 13-bit Barker code has the lowest PSL. This indicates that it has the best suppression effect of pulse compression sidelobes and high SNR. Therefore, 13-bit Barker code is used to encode the carrier signal in this paper.

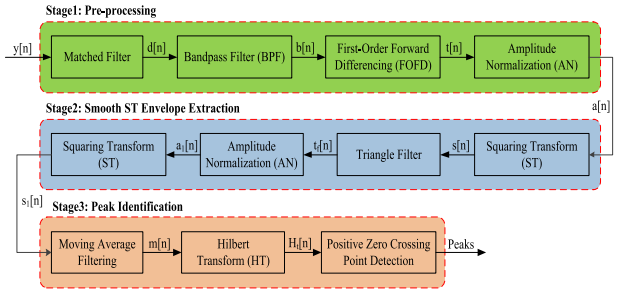

FIGURE 6. Process block diagram of the proposed peak detection algorithm.

C. THE PROPOSED PEAK DETECTION ALGORITHM

The peak detection algorithm has to consider that this type of system must monitor in real-time and be implemented in platforms with reduced resource availability. Fig. 6 shows the process block diagram proposed for the peak detection algorithm. It is composed of three main stages, namely, the pre-processing, the smooth squaring transform (ST) envelope extraction, and the peak identification. The following subsections give a detailed explanation of each stage.

1) SIGNAL PRE-PROCESSING

The signal pre-processing stage is in charge of eliminating noise or some interference. It includes four main steps: the matched filter, bandpass filter (BPF), first-order forward differencing, and amplitude normalization. To adapt the variation of the excitation frequency and satisfy the detection requirement of remote control, a DBTF is designed using a bilinear transform method. The standard transfer function of a second-order analog bandpass filter can be expressed as

$$H(s) = H_{\mathrm{OBP}} \frac{\frac{\omega_0}{Q} s}{s^2 + \frac{\omega_0}{Q} s + \omega_0^2} \tag{14}$$

where $\omega_0 = 2\pi f_0$ denotes the center angular frequency of the bandpass filter, Q is quality factor and $s = j\omega$ represents complex angular frequency; H_{OBP} indicates the bandpass output gain at $\omega = \omega_0$. In this paper, the bandpass output gain H_{OBP} equals one at $\omega = \omega_0$. Using the bilinear transform method, (14) can be transformed as a transfer function $H(z)$ of an infinite impulse response (IIR) digital filter, which has the same performance as the analog bandpass filter. The transform formula is given as:

$$s = \frac{2}{T_s} \frac{1 - z^{-1}}{1 + z^{-1}} \tag{15}$$

Here, T_s represents sample interval and $z = e^{sT_s}$ is a complex variable. By substituting (15) into (14), the transfer function $H(z)$ can be derived as:

$$H(z) = c \frac{1 - z^{-2}}{1 + a_1 z^{-1} + a_2 z^{-2}} \tag{16}$$

To eliminate the frequency distortion from the bilinear transform, a pre-correction process needs to be carried out. These coefficients from (16) are obtained as [30]

$$c = \frac{\tan(\frac{\omega_0 T_s}{2})}{Q + \tan(\frac{\omega_0 T_s}{2}) + Q\tan^2(\frac{\omega_0 T_s}{2})} \tag{17}$$

$$a_1 = \frac{2Q\tan^2(\frac{\omega_0 T_s}{2}) - 2Q}{Q + \tan(\frac{\omega_0 T_s}{2}) + Q\tan^2(\frac{\omega_0 T_s}{2})} \tag{18}$$

$$a_2 = \frac{Q - \tan(\frac{\omega_0 T_s}{2}) + Q\tan^2(\frac{\omega_0 T_s}{2})}{Q + \tan(\frac{\omega_0 T_s}{2}) + Q\tan^2(\frac{\omega_0 T_s}{2})} \tag{19}$$

For the convenience of programming, the transfer function from (16) can be re-expressed as

$$H(z) = c \frac{1 - z^{-2}}{1 + a_1 z^{-1} + a_2 z^{-2}} = \frac{b(z)}{d(z)} \tag{20}$$

Here, $b(z)$ and $d(z)$ represent the output and input for the digital bandpass filter, respectively. Then considering $d\,[n]$ the input sequence of the filter and $b\,[n]$ its output sequence, the following equation can be obtained:

$$b\,[n] + a_1 z^{-1} b\,[n] + a_2 z^{-2} b\,[n] = cd\,[n] - cz^{-2} d\,[n] \tag{21}$$

Based on the shifting property of the bilateral Z transform from (22), (21) can be rewritten as (23).

$$z^{-n} x(k) = x(k - n) \tag{22}$$

$$b[n] = c[d[n] - d[(n-2)]] - a_1 b[n-1] - a_2 b[n-2] \tag{23}$$

where n is the shifting length and has the value of $n = \pm 1, \pm 2, \pm 3 \cdots$.

Thence, in light of (23), the frequency variation of the received signals can be efficiently tracked only by changing three main parameters composing of f_0, Q and T_s. Fig. 7 shows the frequency response of the DBTF for $f_0 = 35$kHz as an example for different values of Q. It can be seen that the filter has a good frequency response within its bandwidth.

To further reduce some interference or low-frequency noise, the first-order forward differencing is used. The differentiation acts as a high-pass filter and it is expressed as

$$t\,[n] = b\,[n+1] - b\,[n] \tag{24}$$

where $b\,[n]$ indicates the output of the DBTF. The output of the differentiator is a bipolar signal and so a rectification is required to simplify the process of peak identification. Then the differentiated signal $t\,[n]$ is normalized using (25) before squaring transform.

$$a\,[n] = norm(t\,[n]) = \frac{t\,[n]}{\max(|t\,[n]|)} \tag{25}$$

where $a\,[n]$ represents the normalized signal.

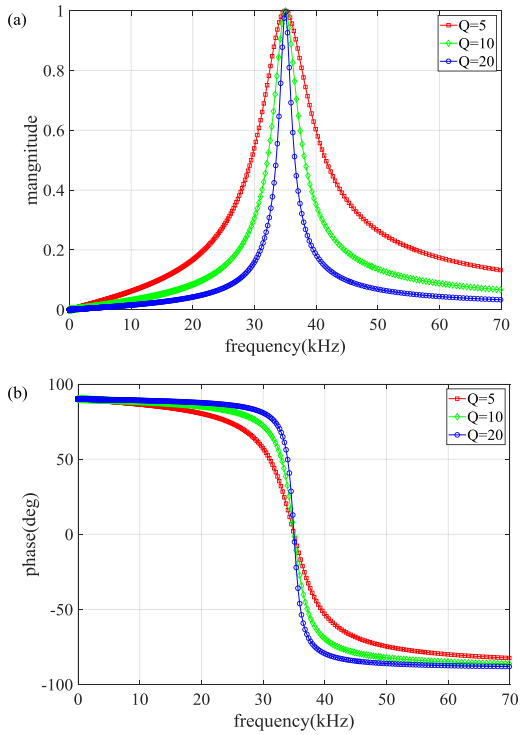

FIGURE 7. The frequency response of a DBTF at f_0=35 kHz, (a) magnitude, (b) phase.

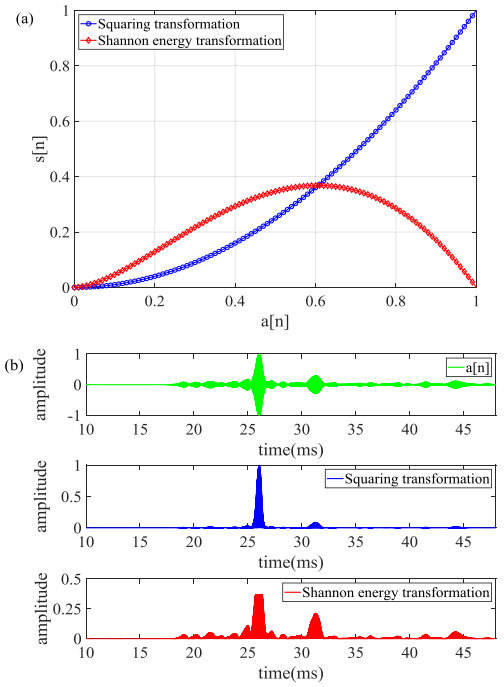

FIGURE 8. The comparison of ST and SET, (a) comparison of energy values, (b) comparison of signal s[n].

2) SMOOTH UNIPOLAR ENVELOPE EXTRACTION

The extraction of the smooth unipolar envelope is to obtain unique positive zero-crossing point in the transformed signal by Hilbert transform (HT). If the extracted envelope is not smooth that has many spikes, this will result in generating extra positive zero-crossing points in the transformed signal. This stage primarily includes squaring transform, triangle filter, amplitude normalization, and moving average (MA) filter. To enhance the mainlobe peak of output results of the matched filter and make the bipolar signal convert to unipolar, a nonlinear transform is required. Squaring transform (ST) and Shannon energy transform (SET) can be a better choice. Their mathematical formulations are given as

$$\text{ST}: \; s[n] = a[n] \cdot a[n] \tag{26}$$

$$\text{SET}: s[n] = -(a[n])^2 \log((a[n])^2) \tag{27}$$

With the aim of choosing a suitable nonlinear transform, the signal $s[n]$ is calculated for ST and SET in Fig. 8a. In Fig. 8a, it can be observed that ST gives a weighted exponential response to the high-intensity components while SET emphasizes medium intensity components. In addition, Fig. 8b shows the result of applying ST and SET to a real measured signal through a matched filter. From Fig. 8b, ST greatly enhances mainlobe peak and decreases sidelobe level compared with SET. Hence, ST is chosen as a nonlinear transform in this work.

After ST, the transformed signal $s[n]$ passes through a triangle filter to obtain a smooth envelope. The triangle filter consists of two cascaded Moving Average (MA) filters. The MA filter acts as a low pass filter, essentially, it is a window-based averaging filter and easy to achieve by programming. The mathematical formulation of MA filters is given as:

$$m[n] = \frac{1}{N_w}\left[\begin{matrix} s(n-(N_w-1)) + s(n-(N_w-2)) \\ + \cdots + s(n) \end{matrix}\right] \tag{28}$$

where N_w denotes the window length. For getting better performance, a suitable selection of the window length is crucial. In general, the window length is taken as much as the mainlobe width of correlation results [24]. If the window length is too small, then it generates multiple envelopes for a single correlation peak, resulting in producing extra positive zero-crossing points in the transformed signal by using HT. On the contrary, it involves some useless information. Finally, the impulse response of the triangle filter $t_f[n]$ can be expressed as:

$$t_f[n] = m[n] * m[n] \tag{29}$$

Here, $*$ represents the convolution operator.

Additionally, the amplitude normalization, squaring transform, and MA filtering from (30), (31), (32), are used for the filtered signal $t_f[n]$ to smoothen the envelope extraction.

$$a_1[n] = \frac{t_f[n]}{\max(|t_f[n]|)} \tag{30}$$

$$s_1[n] = a_1[n] \cdot a_1[n] \tag{31}$$

$$m_1[n] = \frac{1}{N_w}\left[\begin{matrix} s_1(n-(N_w-1)) + s_1(n-(N_w-2)) \\ + \cdots + s_1(n) \end{matrix}\right] \tag{32}$$

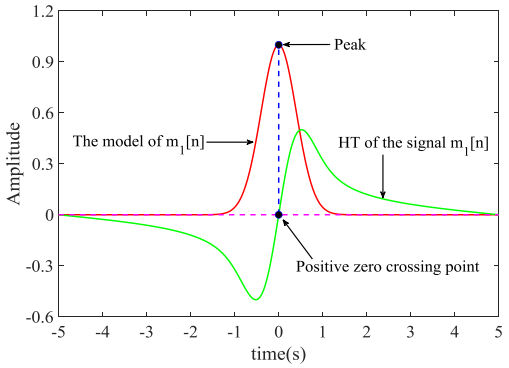

FIGURE 9. Illustration of peak detection by positive zero crossing point.

3) HILBERT TRANSFORM-BASED PEAKS IDENTIFICATION

This stage introduces a novel automatic peak-detection logic exploiting the property of HT. The HT is extensively used in analyzing the instantaneous amplitude and frequency of the signal. The HT definition of a real signal $x(t)$ can be given as [22]

$$\hat{x}(t) = H\left[x(t)\right] = \frac{1}{\pi t} * x(t) = \frac{1}{\pi}\int_{-\infty}^{\infty} \frac{x(\tau)}{t-\tau} d\tau \quad (33)$$

where $*$ indicates the convolution operator. From (33), it can be found that the HT in the time domain is obtained by performing the convolution between the signal $x(t)$ and $1/\pi t$. In the frequency domain, the HT can be expressed as

$$\hat{X}(f) = F\left[\frac{1}{\pi t}\right] \cdot F\left[x(t)\right] = -jsgn(f)X(f) \quad (34)$$

where $X(f)$ is the Fourier transform of the signal $x(t)$, j is the imaginary unit. Then the HT of the signal $x(t)$ can be calculated as:

$$\hat{x}(t) = IFT\left[\hat{X}(f)\right] \text{ where } \begin{cases} \hat{X}(f) = jX(f), f < 0 \\ \hat{X}(f) = -jX(f), f > 0 \end{cases} \quad (35)$$

Here, IFT denotes the inverse Fourier transform.

To illustrate the maxima finding logic using HT, an even Gaussian function is taken as an envelope model because its shape is very similar to an envelope of the signal $m_1\,[n]$. If HT is applied to the Gaussian function the resulting process is shown in Fig. 9. It can be observed that the HT generates a positive zero crossing point in the transformed signal corresponding to a peak of the signal $m_1\,[n]$. Hence, by detecting positive zero-crossing points, the peak of the signal $m_1\,[n]$ can be identified accurately.

Using this technique, there is no need for any amplitude threshold to detect the peaks. After the HT, only by extracting positive zero-crossing points of the transformed signal $H_t\,[n]$, the corresponding peaks of the signal $m_1\,[n]$ are identified.

III. RESULTS AND DISCUSSION

A. THE ANALYSIS OF BARKER CODE

Firstly, a comparison of single-pulse excitation (8 cycles square wave pulse) and Barker coded excitation is performed

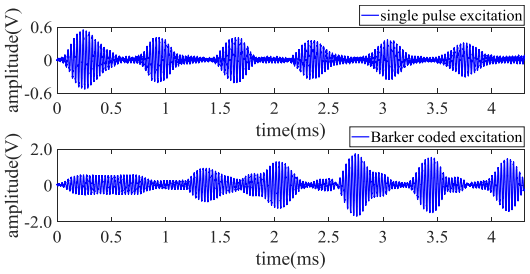

FIGURE 10. The comparison of the received signals for single pulse excitation and Barker coded excitation.

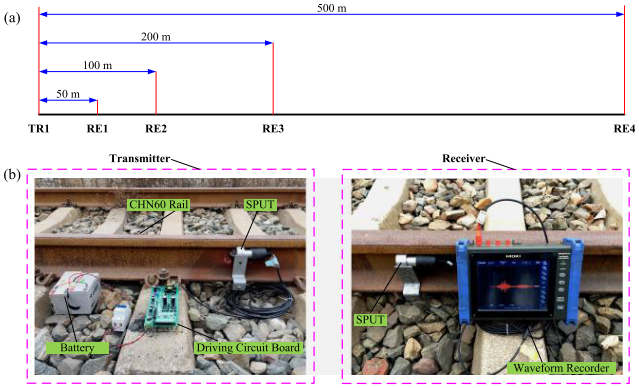

FIGURE 11. The illustration of filed test, (a) schematic diagram, (b) experimental platform based on pitch-catch.

by experiments based on 1 m CHN60 rail in the lab. The excitation voltage is 20 V and the number of carrier cycles is 8 for Barker coded excitation. The comparative result of two excitations is shown in Fig. 10. From Fig. 10, it is found that the amplitude of the received signal is larger when Barker coded excitation is used. The amplitude values of single-pulse excitation and Barker coded excitation are 0.55 V and 1.75 V, respectively. The definition of SNR is given as

$$SNR = 10 \cdot \log_{10}\left(\frac{A_s}{A_n}\right) \quad (36)$$

Here, A_s is the signal amplitude and $A_n = 0.01$V is the noise amplitude. From (36), it is found that SNR of the received signal is increased by 5 dB when Barker coded excitation is used.

Moreover, the selection of carrier cycles, noise performance, and the effect of propagation distance on pulse compression are investigated by utilizing simulations and experiments. The illustration of a field test is shown in Fig. 11. In Fig. 11a, TR1 represents transmitters and REi ($i = 1, 2, 3, 4$) denotes receivers. The test distances include 50 m, 100 m, 200 m, and 500 m. A pitch-catch experimental platform is established in Fig. 11b, which consists of SPUTs, batteries, CHN60 Rail, driving circuit board, and waveform recorder MR8875-30 (HIOKI E.E. CORPORATION). Here, the driving circuit board is used to excite SPUTs, which is designed based on full-bridge topology. The waveform recorder saves the data from received signals.

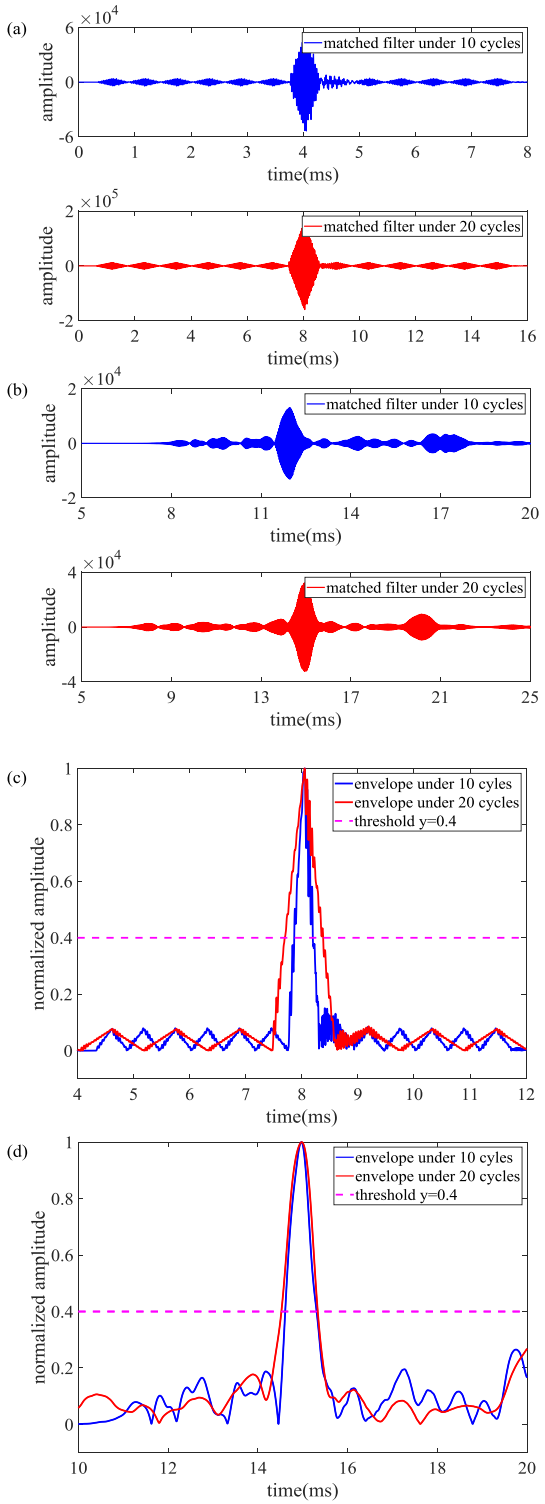

FIGURE 12. The comparison of simulated and measured results, (a), (b) matched filtering under 10 and 20 cycles, (c), (d) normalized envelopes comparison under 10 and 20 cycles.

1) THE SELECTION OF CARRIER CYCLES OF BARKER CODE MODULATION

A square wave is chosen as a carrier to reduce the complexity and cost of the hardware. The carrier frequency is 35 kHz in this system. For the detection of breakages in long rails, the number of carrier cycles takes values of 10 and 20 to ensure the UGW signal received by a receiver. Based on the PSpice model of the pitch-catch setup from Fig. 2 and the experimental platform from Fig. 11b, the effect of the number of carrier cycles on pulse compression is analyzed when the rail length is 50 m. Fig. 12a and Fig. 12b present the simulated and measured pulsed compression results, respectively, for 10 and 20 carrier cycles. The main lobe peak is greatly increased with 20 cycles compared with the case of using only 10 cycles. Fig. 12c and Fig. 12d shows the corresponding normalized envelopes. It is seen that the larger number of carrier cycles, the larger MLW and the lower PSL. It is also shown that the simulated results are in agreement with the measured ones. Note that a small MLW and low PSL are required to guarantee good range resolution and high SNR in practice. If carrier cycles keep increasing, MLW and the duration of the received signal will be increased, which leads to taking more time to process the received signal and decreasing range resolution. Therefore, the number of carrier cycles will take 20 in this study.

The difference between the simulated results and the measured ones can be well explained as follows. Firstly, SPUTs in the PSpice model are built based on one-dimensional wave and transmission line theories, but the radial mode exists in practice. Furthermore, the rail in the PSpice model is achieved by using a lossy transmission line. Finally, SPUTs used to transmit and receive signals are identical in the PSpice model while this is very difficult to achieve in practice.

2) THE PERFORMANCE OF THE BARKER CODE WITH NOISE

The detection equipment of broken rails is often in a high noise environment. In general, high SNR is required in the detection. Hence, the analysis of the performance of the Barker code with noise is necessary. The test distance used is 50 m and the number of carrier cycles is 20. Gaussian noises with SNR$=-10$ dB and -20 dB are added to the measured received signals. In this situation, the received signals cannot be distinguished in the received transmissions, as can be seen in Fig. 13. Nevertheless, after matched filtering, the correct correlation peak can still be found. It is concluded that 13-bit Barker code has a strong immunity to noise, which can well satisfy the requirements of the broken rail detection system.

3) THE EFFECT OF PROPAGATION DISTANCE OF UGW ON PULSE COMPRESSION

The dispersion and multimode transmission of UGW are closely related to the geometry shape of structures and to the propagation distances. For this reason, the analysis of the effect of the propagation distance on the pulse compression is carried out. The number of carrier cycles is 20 and the test distances are 50 m, 100 m, 200 m, and 500 m, respectively. The corresponding normalized envelopes are extracted in Fig. 14a and the MLW and PSL are calculated and presented in Fig. 14b, to conveniently compare pulse compression results under different propagation distances.

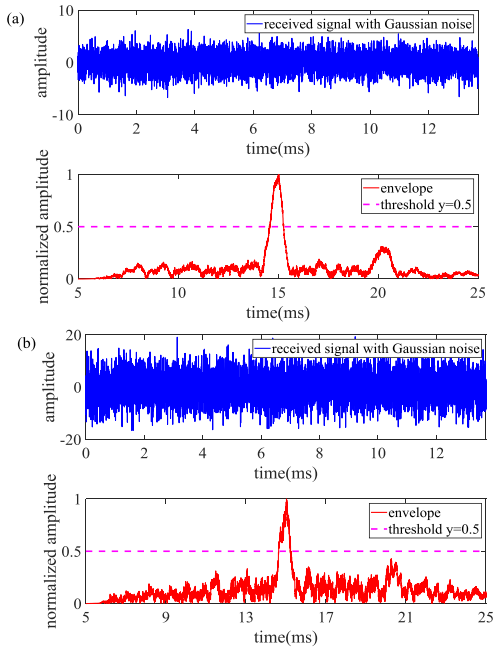

FIGURE 13. The analysis of noise performance of Barker code, (a) SNR=−10 dB, (b) SNR=−20 dB.

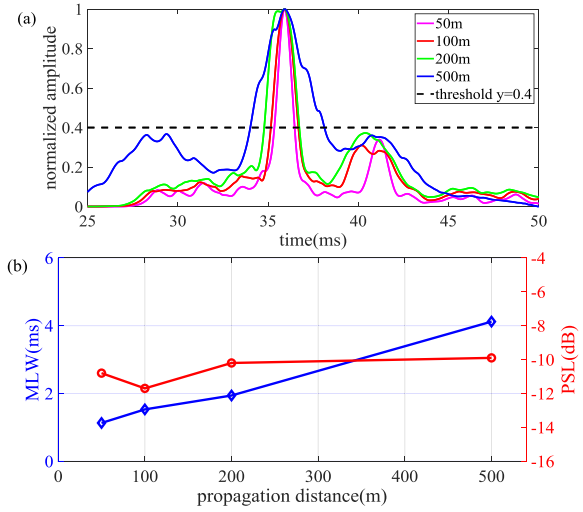

FIGURE 14. The comparison of pulse compression results under different propagation distances, (a) normalized envelopes comparison, (b) MLW and PSL.

According to Fig. 14, with the increase of propagation distances, MLW increases linearly while PSL is almost unchanged.

The reason is that the dispersion of UGW can cause the wave-packets to spread out in space and time as it propagates through structures. Additionally, the duration of the wave-packet increases linearly with the propagation distance [31]. All that limits the range resolution that can be obtained in a long-range detection system based on UGW.

B. THE ANALYSIS OF THE PROPOSED PEAKS DETECTION ALGORITHM

In order to validate the accuracy and stability of the proposed peaks detection algorithm, the real measured signals are analyzed under different window lengths of MA filter and propagation distances, adding Gaussian noise with SNR=-20 dB. The specific analysis is detailed in the subsections below.

1) THE EFFECT OF THE WINDOW LENGTH OF THE MA FILTER ON PEAK DETECTION

The smooth envelope is obtained by using a triangle filter, which is composed of two cascaded MA filters. The smooth envelope is crucial for the achievement of positive zero-crossing points by using HT. Here, the analysis of the effect of the window length N_w of the MA filter on peak detection is conducted, for the case of 20 carrier cycles and a test distance of 500 m. In this case, the mainlobe width of the pulse compression result is around 2.4 ms and the sampling frequency is 500 kHz, so the mainlobe width, in samples, is 1200. Consequently, the window lengths considered are $N_w = 100, 1200, 2000$ samples, respectively.

Fig. 15 presents the peak detection results under these different window lengths. Fig. 15a shows that the signal after the triangle filter generates multi-peaks when the window length is $N_w = 100$ samples. This leads to the appearance of unexpected positive zero-crossing points. In addition, it can be observed that if the peak value of the filtered signal $t_f[n]$ is small, the positive zero-crossing point cannot appear by using HT. Considering also the results of Fig. 15b and Fig. 15c, only one positive zero-crossing point is obtained when the window length is $N_w = 1200, 2000$ samples, respectively. Besides, the normalized envelopes of the filtered signal $t_f[n]$ under the three window lengths are compared in Fig. 15d. It is shown that, compared to $N_w = 1200$ samples, the peak of the envelope will generate a larger shift if $N_w = 2000$ samples. This leads to some time difference in identifying the received transmissions. Hence, the window length of the MA filter selected is normally equal to the mainlobe width of the pulse compression results.

2) THE DETECTION OF PEAKS UNDER DIFFERENT PROPAGATION DISTANCES

Through the above analysis in subsection *B.1*, it is shown that as long as the window length of the MA filter is similar to the mainlobe width of the pulse compression results, only one positive zero-crossing point is obtained. In this section, the performance of the proposed peak detection method for different distances is analyzed. Note that the number of carrier cycles is unchanged regarding the previous subsection *B.1* and the test distances considered are 50 m, 100 m, 200 m, and 500 m, respectively.

Fig. 16 presents the peak detection results under different test distances, showing that only one positive zero-crossing point is obtained for all the test distances. Furthermore, it is also shown that small peaks in the filtered signal $t_f[n]$ have no influence on the extraction of positive zero-crossing points. These results can well demonstrate that the proposed method for the detection of peaks has strong robustness.

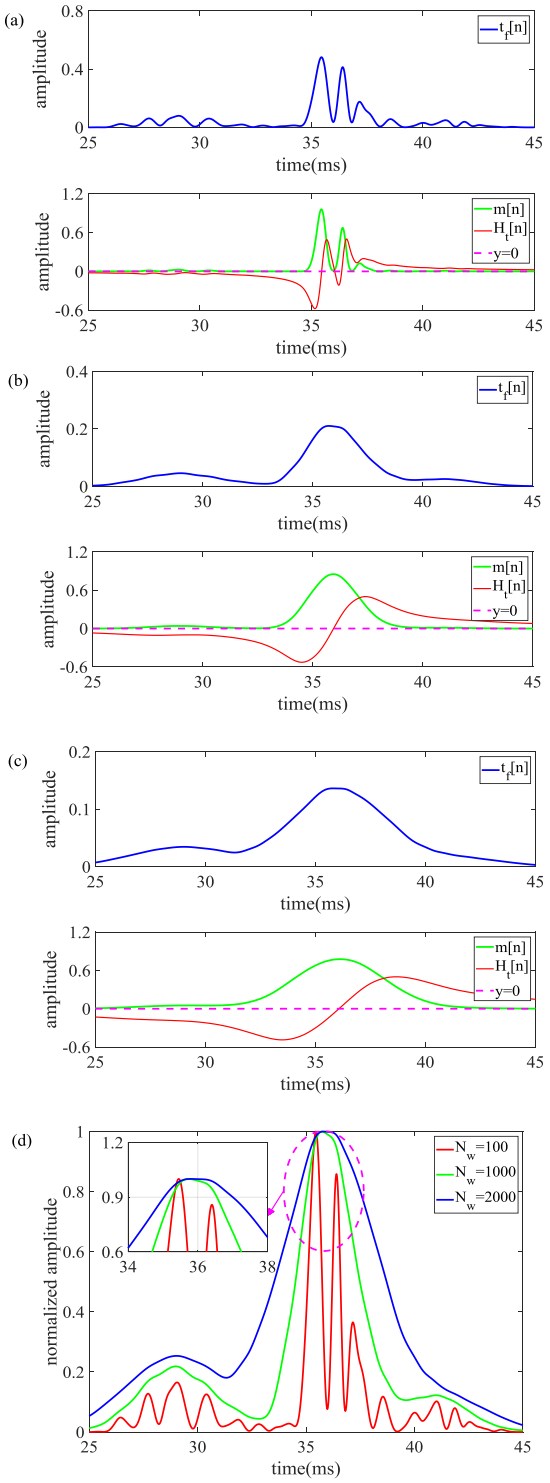

FIGURE 15. The analysis of the effect of the window length of the MA filter on the peak detection, (a) Nw =100, (b) Nw =1200, (c) Nw =2000, (d) comparison of normalized envelopes.

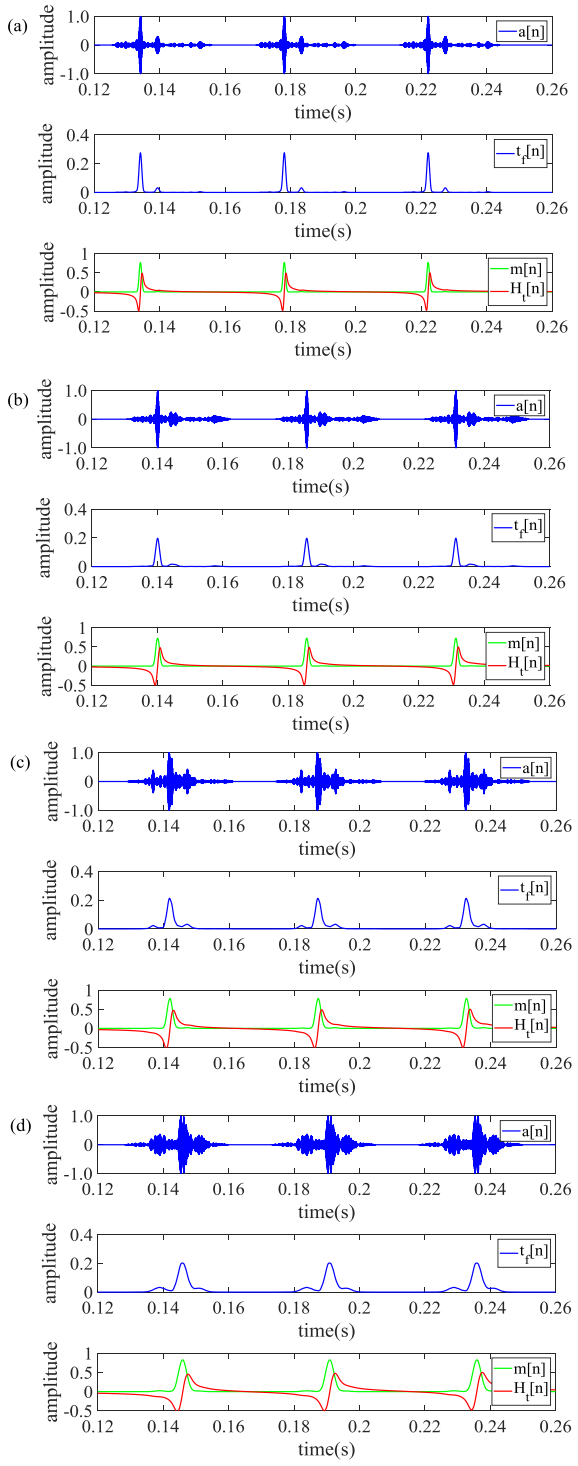

FIGURE 16. The analysis of peak detection under different test distances, (a) 50 m, (b) 100 m, (c) 200 m, (d) 500 m.

3) THE DETECTION OF PEAKS UNDER ADDING GAUSSIAN NOISE AND DIFFERENT PROPAGATION DISTANCES

Strong immunity to noise is required for a real-time broken rail detection system, especially in the detection of breakages for long rails in service. Gaussian noises with SNR=−20 dB are added in the received signals of different test distances.

As can be seen in Fig. 17, after the proposed processing, including filtering, envelope extraction, and HT, the positive zero-crossing points corresponding to the mail peaks are obtained under the different test distances. It is shown that the proposed peak detection algorithm has strong anti-noise performance. With the increase of the propagation distance,

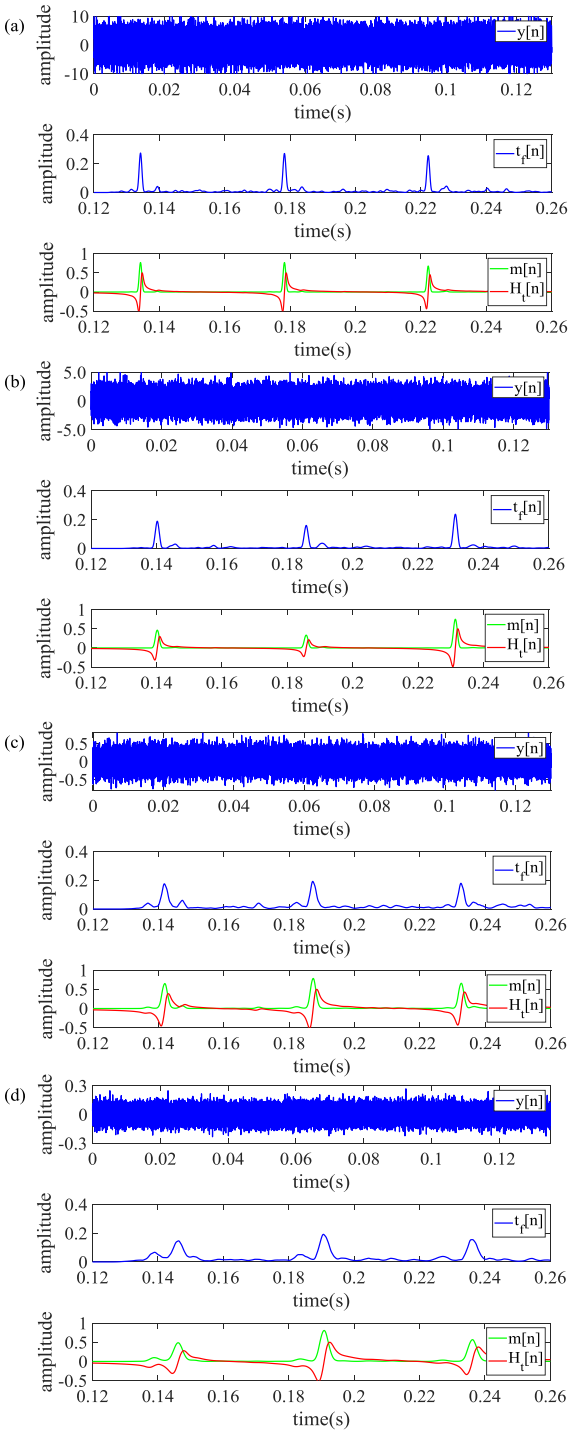

FIGURE 17. The analysis of peak detection results under Gaussian noise with SNR=−20dB, (a) 50 m, (b) 100 m, (c) 200 m, (d) 500 m.

the influence of the dispersion of UGW on MLW is gradually increasing. Note that the lower the MLW, the higher the range resolution.

4) COMPARATIVE ANALYSIS OF THE PROPOSED PEAK DETECTION ALGORITHM AND THE PREVIOUS WORKS

The comparison of the proposed peak detection algorithm and the novel adaptive peak detection method proposed in [24]

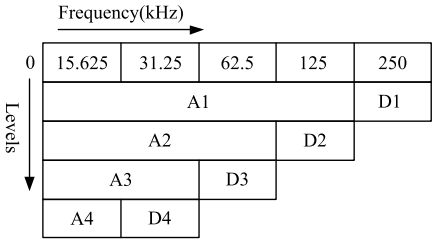

FIGURE 18. The scheme of DWT decomposition of the UGW signal.

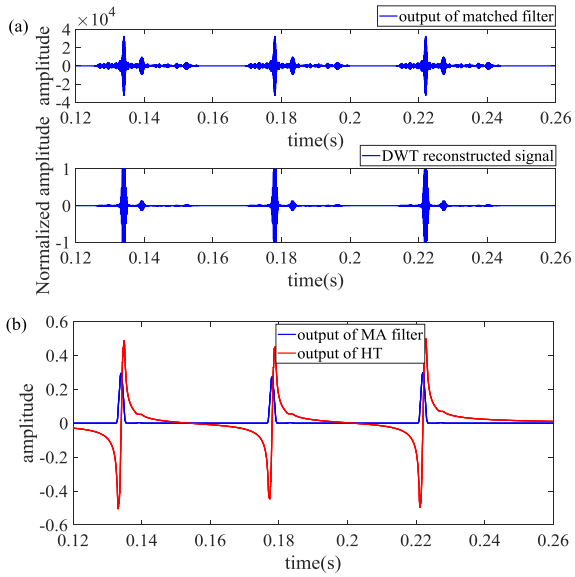

FIGURE 19. The analysis of peak detection algorithm based DWT for the case of 20 carrier cycles and a test distance of 50 m, (a) DWT reconstructed signal, (b) peak detection results by using HT.

is performed. This peak detection method is mainly based on the discrete wavelet transform (DWT), on a moving average filter, as well as on the Hilbert Transform. Generally, the selection of appropriate wavelet has a great influence on the performance of signal processing algorithms based on wavelet transform. It should be noted that the choice of wavelet is only application dependent. In this work, *db1* wavelet is used to decompose into four levels. According to Nyquist's rule($(f_s \geq 2f_m)$ where f_s represents the sample rate and f_m is the highest frequency of the signal), the frequency components of the Barker coded UGW signal will be in the range of 0 Hz-250 kHz. A specific description of the frequency range of each level decomposition is presented in Fig. 18. The frequency of Barker coded excitation is 35 kHz, from Fig. 18, the detail coefficients of D3 and D4 can capture this frequency information. Then the reconstruction operation is performed by D3 and D4.

Fig. 19 and Fig. 20 show the peak detection results of two peak detection algorithms. From Fig. 19b and Fig. 20b, it is obvious that the two peak detection algorithms can accurately identify the peaks. In addition, compared to the peak detection method based on DWT [24], the signal amplitude through the MA filter is larger for the proposed peak detection algorithm. The total processing time for two peak detection

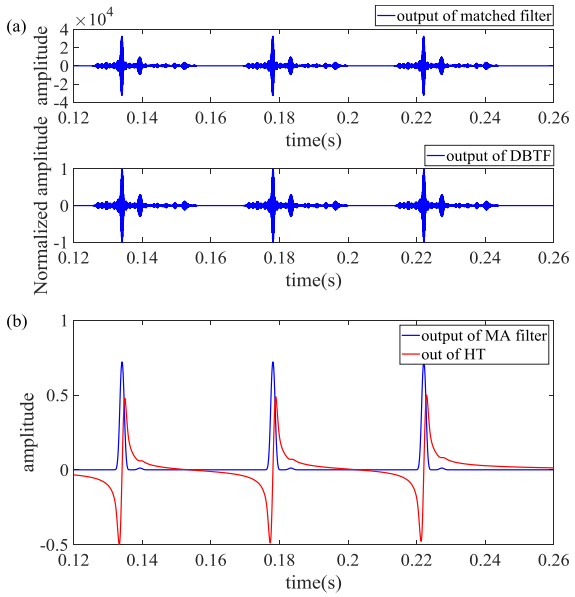

FIGURE 20. The analysis of peak detection algorithm based DBTF for the case of 20 carrier cycles and a test distance of 50 m, (a) filtered signal by using DBTF, (b) peak detection results by using HT.

TABLE 3. The comparison of processing time for the peak detection method based on DWT [24] and this work.

Parameters	Total time (s)	DWT (s)	DBTF (s)
The peak detection method [24]	0.405	0.122s	-
This work	0.325s	-	0.008s

methods and the processing time of DWT and DBTF are calculated by using the following platform:

- Processer and RAM: Inter (R) Core (TM) i7-5500U CPU @ 2.4 GHz, 8 GB;
- Operation system: 64-bit Windows 7;
- Analysis software: MATLAB 9.7.

These time values are listed in Table 3. According to Table 3, the total processing time of the proposed peak detection algorithm is shorter.

In order to perform further comparison for two peak detection methods, four performance factors [23] namely, sensitivity (Se), positive predictivity (+P), error rate (Er), accuracy (Acc) are used in this work. The definition of these factors is given as

$$Se = \frac{TP}{TP + FN} \tag{37}$$

$$+P = \frac{TP}{TP + FP} \tag{38}$$

$$Er = \frac{FP + FN}{TP} \tag{39}$$

$$Acc = \frac{TP}{TP + +FN + FP} \tag{40}$$

Here, TP is the number of correctly detected peaks, FN is the number of missed peaks, and FP is the number of false peaks. The Gaussian noise with SNR $= -20$ dB is added in the received signals under the test distances of 100 m, 200 m, and 500 m. For each of the above cases, TP, FN, and FP are counted for 10 times peak detection results. The performance comparison of two peak detection methods for every case is listed in Table 4, Table 5, and Table 6. According to Table 4, Table 5, and Table 6, it can be concluded that the performance of the proposed peak detection algorithm is superior.

TABLE 4. The performance comparison of the peak detection method [24] and this work for the case of 20 carrier cycles and a test distance of 100 m, Gaussian noise SNR=−20 dB.

parameters	TP	FP	FN	Se (%)	+P (%)	Er (%)	Acc (%)
The peak detection method [24]	30	4	0	100	88.24	13.33	88.24
This work	30	1	0	100	96.77	3.33	96.77

TABLE 5. The performance comparison of the peak detection method [24] and this work for the case of 20 carrier cycles and a test distance of 200 m, Gaussian noise SNR=−20 dB.

parameters	TP	FP	FN	Se (%)	+P (%)	Er (%)	Acc (%)
The peak detection method [24]	30	6	0	100	83.33	20	83.33
This work	30	4	0	100	88.24	13.33	88.24

TABLE 6. The performance comparison of the peak detection method [24] and this work for the case of 20 carrier cycles and a test distance of 500 m, Gaussian noise SNR=−20 dB.

parameters	TP	FP	FN	Se (%)	+P (%)	Er (%)	Acc (%)
The peak detection method [24]	30	7	0	100	81.08	23.33	81.08
This work	30	4	0	100	88.24	13.33	88.24

In general, the power of a broken rail detection system based on UGW is supplied by using solar energy. Hence, the processing algorithm should be simple as soon as possible which is conducive to saving energy. In summary, compared to the previous works, the proposed peak detection algorithm has the following advantages:

- Not requiring any amplitude threshold;
- Less time cost;
- It is suitable for other encoding transmissions;
- It is easy to accomplish by programming;
- It is easy to integrate into a real-time detection system;

However, to sufficiently exploit the pulse compression technique and improve range resolution, compensation of dispersion of UGW is essential. In addition, it can be found that the mainlobe width of pulse compression results is a prerequisite for the decision of window length of the MA filter, so the online calculation of the mainlobe width of pulse compression results is necessary. These will be expected to further investigate in subsequent work.

IV. CONCLUSION

In this work, Barker coded UGW signals are analyzed by simulations using a PSpice model of a pitch-catch setup

and by real experimentations with a test platform of pitch-catch. Based on the aforementioned encoded transmissions, an adaptive peak detection algorithm without any amplitude threshold is proposed by DBTF, MA filter, and HT. To validate the accuracy and robustness of the proposed peak detection method, the measured signals under Gaussian noise with SNR=−20 dB and different test distances from 50 m to 500 m are analyzed. In summary, according to the above analysis, the following conclusions can be obtained:

(1) It is shown that Barker coded UGW signals can efficiently improve SNR by 5 dB and have a strong immunity to noise. For 13-bit Barker code, with the increase of the number of carrier cycles, PSL is decreased while MLW is improved. However, as the detection distance increases, MLW is linearly increased while PSL is basically unchanged. In addition, 13-bit Barker code modulated using 20 carrier cycles can well satisfy requirements of SNR and range resolution of the detection of breakages in long rails.

(2) The window length of the MA filter has a great influence on the extraction of positive zero-crossing points for peak detection using HT. When the window length is too small, unexpected positive zero-crossing points will appear. On the other hand, the maximum peak of the envelope of the filtered signal $t_f[n]$ will generate shift when the window length is too large. Hence, the window length of the MA filter is normally selected similar to the mainlobe width of the pulse compression results.

(3) It is shown that compared to the previous works, the proposed adaptive peak detection algorithm has stronger robustness and better anti-noise performance. Additionally, it is easy to accomplish by programming and to integrate into a real-time detection system. To improve the performance of the proposed peak detection algorithm, online measurement of window length of the MA filter and the dispersion compensation of UGW in long rails will be investigated in future works.

REFERENCES

[1] J. Li, Y. Lu, R. Guan, and W. Qu, "Guided waves for debonding identification in CFRP-reinforced concrete beams," *Construct. Building Mater.*, vol. 131, pp. 388–399, Jan. 2017.

[2] A. R. P. Dias, C. Nageswaran, R. C. Jacques, and T. G. R. Clarke, "Medium range guided wave inspection of the triple point in lined pipes by EMATs," *J. Nondestruct. Eval.*, vol. 38, no. 3, Sep. 2019.

[3] X. Xining, Z. Lu, X. Bo, Y. Zujun, and Z. Liqiang, "An ultrasonic guided wave mode excitation method in rails," *IEEE Access*, vol. 6, pp. 60414–60428, 2018.

[4] L. Yuan, Y. Yang, Á. Hernández, and L. Shi, "Feature extraction for track section status classification based on UGW signals," *Sensors*, vol. 18, no. 4, p. 1225, 2018.

[5] I. I. Setshedi, P. W. Loveday, C. S. Long, and D. N. Wilke, "Estimation of rail properties using semi-analytical finite element models and guided wave ultrasound measurements," *Ultrasonics*, vol. 96, pp. 240–252, Jul. 2019.

[6] X. Wei, Y. Yang, and N. Yu, "Research on broken rail real-time detection system for ultrasonic guided wave," in *Proc. Int. Conf. Electromagn. Adv. Appl. (ICEAA)*, Verona, Italy, Sep. 2017, pp. 906–909.

[7] Y. Yang, X. Wei, L. Zhang, and W. Yao, "The effect of electrical impedance matching on the electromechanical characteristics of sandwiched piezoelectric ultrasonic transducers," *Sensors*, vol. 17, no. 12, p. 2832, 2017.

[8] D. A. Ramatlo, D. N. Wilke, and P. W. Loveday, "Development of an optimal piezoelectric transducer to excite guided waves in a rail Web," *NDT&E Int.*, vol. 95, pp. 72–81, Apr. 2018.

[9] X. Wei, Y. Yang, W. Yao, and L. Zhang, "Design of full bridge high voltage pulser for sandwiched piezoelectric ultrasonic transducers used in long rail detection," *Appl. Acoust.*, vol. 149, pp. 15–24, Jun. 2019.

[10] P. D. Wilcox, M. Lowe, and P. Cawley, "A rapid signal processing technique to remove the effect of dispersion from guided wave signals," *IEEE Trans. Ultrason., Ferroelectr., Freq. Control*, vol. 50, no. 4, pp. 419–427, Apr. 2003.

[11] C.-B. Xu, Z.-B. Yang, X.-F. Chen, S.-H. Tian, and Y. Xie, "A guided wave dispersion compensation method based on compressed sensing," *Mech. Syst. Signal Process.*, vol. 103, pp. 89–104, Mar. 2018.

[12] H. Zhang, S. Wu, D. Ta, K. Xu, and W. Wang, "Coded excitation of ultrasonic guided waves in long bone fracture assessment," *Ultrasonics*, vol. 54, no. 5, pp. 1203–1209, Jul. 2014.

[13] J. Fu, G. Wei, Q. Huang, F. Ji, and Y. Feng, "Barker coded excitation with linear frequency modulated carrier for ultrasonic imaging," *Biomed. Signal Process. Control*, vol. 13, pp. 306–312, Sep. 2014.

[14] L. De Marchi, A. Perelli, and A. Marzani, "A signal processing approach to exploit chirp excitation in Lamb wave defect detection and localization procedures," *Mech. Syst. Signal Process.*, vol. 39, nos. 1–2, pp. 20–31, Aug. 2013.

[15] M. K. Yucel, S. Fateri, M. Legg, A. Wilkinson, V. Kappatos, C. Selcuk, and T.-H. Gan, "Coded waveform excitation for high-resolution ultrasonic guided wave response," *IEEE Trans. Ind. Informat.*, vol. 12, no. 1, pp. 257–266, Feb. 2016.

[16] H. Li and Z. Zhou, "Application of P4 polyphase codes pulse compression method to air-coupled ultrasonic testing systems," *Ultrasonics*, vol. 78, pp. 57–69, Jul. 2017.

[17] L. Yuan, Y. Yang, and Á. Hernández, "Improvement of high-voltage impulses in track circuits with kasami and LS codes," *Int. J. Circuit Theory Appl.*, vol. 46, no. 4, pp. 926–941, Apr. 2018.

[18] R. J. Hill, "Optimal construction of synchronizable coding for railway track circuit data transmission," *IEEE Trans. Veh. Technol.*, vol. 39, no. 4, pp. 390–399, Nov. 1990.

[19] F. Filippone, A. Mariscotti, and P. Pozzobon, "The internal impedance of traction rails for DC railways in the 1–100 kHz frequency range," *IEEE Trans. Instrum. Meas.*, vol. 55, no. 5, pp. 1616–1619, Oct. 2006.

[20] R. Escudero, A. Hernandez, M. C. Perez, J. M. Villadangos, C. Diego, and J. Urena, "Local maximum detection for active sensory systems based on encoding and correlation techniques," in *Proc. IEEE Int. Instrum. Meas. Technol. Conf. Proc.*, Graz, Austria, May 2012, pp. 1697–1702.

[21] R. Gutierrez-Rivas, J. J. Garcia, W. P. Marnane, and A. Hernandez, "Novel real-time low-complexity QRS complex detector based on adaptive thresholding," *IEEE Sensors J.*, vol. 15, no. 10, pp. 6036–6043, Oct. 2015.

[22] M. S. Manikandan and K. P. Soman, "A novel method for detecting R-peaks in electrocardiogram (ECG) signal," *Biomed. Signal Process. Control*, vol. 7, no. 2, pp. 118–128, Mar. 2012.

[23] M. Rakshit and S. Das, "An efficient wavelet-based automated R-peaks detection method using Hilbert transform," *Biocybern. Biomed. Eng.*, vol. 37, no. 3, pp. 566–577, 2017.

[24] L. Yuan, Y. Yang, Á. Hernández, and L. Shi, "Novel adaptive peak detection method for track circuits based on encoded transmissions," *IEEE Sensors J.*, vol. 18, no. 15, pp. 6224–6234, Aug. 2018.

[25] L. Galloy, L. Berquez, F. Baudoin, and D. Payan, "PSpice modeling of the pulsed electro-acoustic signal," *IEEE Trans. Dielectr. Electr. Insul.*, vol. 21, no. 3, pp. 1143–1153, Jun. 2014.

[26] X. Wei, Y. Yang, W. Yao, and L. Zhang, "PSpice modeling of a sandwich piezoelectric ceramic ultrasonic transducer in longitudinal vibration," *Sensors*, vol. 17, no. 10, p. 2253, 2017.

[27] J. Lin, J. Hua, L. Zeng, and Z. Luo, "Excitation waveform design for Lamb wave pulse compression," *IEEE Trans. Ultrason., Ferroelectr., Freq. Control*, vol. 63, no. 1, pp. 165–177, Jan. 2016.

[28] T. H. Gan, D. A. Hutchins, D. R. Billson, and D. W. Schindel, "The use of broadband acoustic transducers and pulse-compression techniques for air-coupled ultrasonic imaging," *Ultrasonics*, vol. 39, no. 3, pp. 181–194, Apr. 2001.

[29] H. Zhao, L. L. Mo, and S. Gao, "Barker-coded ultrasound color flow imaging: Theoretical and practical design considerations," *IEEE Trans. Ultrason., Ferroelectr., Freq. Control*, vol. 54, no. 2, pp. 319–331, Feb. 2007.

[30] X. Wei, Y. Yang, W. Yao, and L. Zhang, "An automatic optimal excitation frequency tracking method based on digital tracking filters for sandwiched piezoelectric transducers used in broken rail detection," *Measurement*, vol. 135, pp. 294–305, Mar. 2019.
[31] P. Wilcox, M. Lowe, and P. Cawley, "The effect of dispersion on long-range inspection using ultrasonic guided waves," *NDT&E Int.*, vol. 34, no. 1, pp. 1–9, Jan. 2001.

XIAOYUAN WEI received the B.S. degree from Northwest Normal University, in 2012, and the M.S. degree from the Xi'an University of Technology, in 2015. He is currently a Co-Supervised Ph.D. Student with the Xi'an University of Technology and the University of Alcalá. His main research interests are ultrasonic guided wave detection and structural health monitoring.

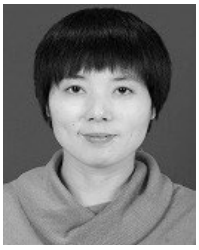

YUAN YANG received the B.S., M.S., and Ph.D. degrees from the Xi'an University of Technology, China, in 1997, 2000, and 2004, respectively. From 2000 to 2004, she was a Lecturer, and from 2004 to 2009, she was an Assistant Professor. In 2004, she held her research at Kyushu University, Japan, as a Visiting Scholar. Since 2009, she has been a Professor with the Electronics Department, Xi'an University of Technology. She took charge of three projects at the National Natural Science Foundation of China, ten public-funding projects, and 20 projects with industry. She has published more than 70 articles. Her main research interests include the digital-analog mixed integrated circuit design and the design of track circuit systems.

JESÚS UREÑA (Senior Member, IEEE) received the B.S. degree in electronics engineering and the M.S. degree in telecommunications engineering from the Universidad Politécnica de Madrid, Madrid, Spain, in 1986 and 1992, respectively, and the Ph.D. degree in telecommunications from the Universidad de Alcalá, Alcalá de Henares, Spain, in 1998. Since 1986, he has been with the Department of Electronics, University of Alcalá, where he is currently a Professor. His current research interests are in the areas of ultrasonic signal processing, local positioning systems (LPSs), and distributed sensory systems for smart spaces and intelligent transportation.

JIAXUAN YAN received the B.S. degree from Nanjing Tech University, in 2018. He is currently pursuing the M.S. degree with the Xi'an University of Technology. His main research interest is the modeling of ultrasonic guided waves detection rail channel.

HAOZHEN WANG received the B.S. degree from the Shaanxi University of Technology, in 2007. She is currently pursuing the M.S. degree with the Xi'an University of Technology. Her main research interest is ultrasonic guided wave detection.